Designing a dual-core photonic crystal fiber coupler by means of microfluidic infiltration

F. Koohi-Kamali[a], M. Ebnali-Heidari[b], and M.K. Moravvej-Farshi[c] *

[a]Department of Electrical Engineering, Science and Research Branch, Islamic Azad University, Tehran 1477893855, Iran
[b]Faculty of Engineering, Shahrekord University, Shahrekord 8818634141, Iran
[c]Faculty of Electrical and Computer Engineering, Advanced Devices Simulation Lab, P.O. Box 14115-149, Tehran 1411713116, Iran

***Corresponding author:** farshi_k@modares.ac.ir

ABSTRACT— We report the results of our study on the role of microfluidic infiltration technique in improving the coupling characteristics of dual-core photonic crystal fiber (PCF) couplers. Using the finite element method (FEM), we evaluate the effective mode area, dispersion and coupling parameters of an infiltrated dual-core PCF. We use these parameters to design a compact and reconfigurable coupler by solving a set of coupled generalized nonlinear Schrödinger equations. This approach allows one to obtain wavelength-flattened dispersion characteristics with bandwidth of 0.8 μm **in the ITU region, and large walk-off length simply by choosing a suitable infiltrated refractive index. We also demonstrate that under certain conditions one can observe a pulse break-up effect to generate pulse trains with high repetition rate.**

KEYWORDS: optical coupler, dispersion engineering, dual-core photonic crystal fiber, dual-core, optofluidic, finite element method, coupled generalized nonlinear Schrödinger equations.

I. INTRODUCTION

In the last two decades, the optical fiber technology has revolutionized the telecommunication industry. In particular, there has been a growing interest in photonic crystal fiber (PCF) in context of all optical devices and more generally for nonlinear optics. A PCF also called micro-structured optical fiber or holey fiber is a novel optical fiber that guides light by single material with an ordered array of air holes running along its length [1]. Compared to conventional optical fiber, PCF offers remarkable features such as no cut-off single-mode transmission, flexible dispersion and high nonlinearity [2]. The PCF coupler is one of the numerous PCF based devices that are the key component for future optical networks. Realization of multi-core, specifically, dual-core PCFs has enabled a new efficient way of designing PCF couplers [3-6], wavelength multiplexers and demultiplexers [7], polarization splitters [8], narrow bandpass filters [9], and sensors [10]. Dual-core PCF couplers have many advantages over the conventional optical couplers. They are more flexible to design, easy to make, and have shorter coupling length. However, most of the proposed techniques to design and fabricate dual-core PCF couplers, so far, are based on varying the PCF geometrical parameters; such as the shape and the size of PCF air-holes [11, 12], These techniques depend on the technological capability to realize a specific design with high precision, and also are limited by the size of the PCF cross-sectional area. In particular, it is quite difficult to control the accurate positions and radii of the air-holes within the PCF lattice. The recent advances in design and preparation of selectively infiltrated PhCs [13-16] and PCFs [17-22], have demonstrated the potential of optofluidics

as an alternative approach in designing and fabrication of PhC- and PCF-based optical devices whose characteristics including dispersion profiles are tailored as desired, without the need to alter the device topology.

In this paper, we propose a reconfigurable microfluidic infiltrated dual-core PCF coupler with nearly zero and ultra-flattened dispersion. The rest of the paper is organized as follows. In Section II, we present the basic idea of the proposed device. Then, in Sections III-V the mathematical analysis of pulse propagation in dual-core PCF and the role of microfluidic infiltration in the proposed approach are discussed. Finally, we will conclude our investigation in Section VI.

II. Physical Structure and Coupling Mechanism of Dual-Core PCF

A 3-D schematic view of the dual-core PCF, under study, is shown in Fig. 1. The structure consists of air-holes assumed to be devised along a pure silica fiber, arranged in a triangular lattice of pitch Λ=2μm. The air-hole diameters are also assumed to be d=0.6Λ. As illustrated in this figure, the two identical cores, "A" and "B" that are separated by one air hole are formed by two missing air-holes. As also depicted in the figure, the PCF optical axis (the propagation direction) is taken along the z-coordinate and the transverse direction falls within the x-y plane.

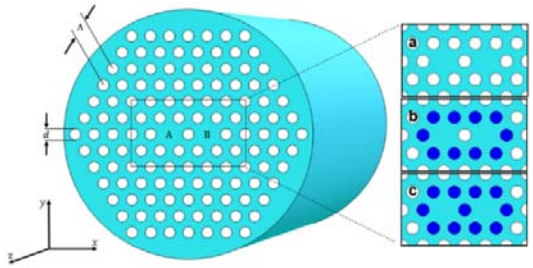

Fig. **1** (a) 3-D schematic view of the dual-core PCF formed by air-holes (white circles) arranged in a triangular lattice of pitch $\Lambda = 2$ μm and diameters of $d = 0.6\Lambda$. (b) and (c) depict the selective infiltration schemes (darker circles represent the infiltrated air-holes).

To calculate the dual-core PCF coupler characteristics, we use vectorial finite element method (FEM) for solving the electromagnetic wave propagation that is described by the Maxwell equations [23].

$$\nabla \times \left(\frac{1}{\mu_r} \nabla \times \mathbf{E} \right) - k_0^2 \varepsilon_r \mathbf{E} = 0 \qquad (1)$$

where ε_r and μ_r are the permittivity and permeability of the materials in the waveguide, respectively, $k_0 = \left(\omega^2 \mu_0 \varepsilon_0\right)^{1/2}$ is the free space wave number, and **E** is the electric field. The wavelength dependence of the permittivity for the silica glass to that can be expressed Sellmeier expansion is given in [24]. Perfectly matched layer (PML) boundary condition is employed at the edges of the computational window in order to account for the leakage property of the modes. Equation (1) describes the waveguide modes that can be solved as an eigenvalue problem by a standard solution in the form of $E = E(x, y)\mathrm{e}^{-i\beta z}$.

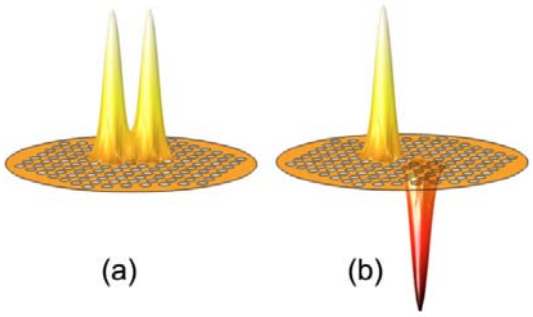

Fig. **2** Calculated (a) even and (b) odd modes propagating along the un-infiltrated dual-core PCF.

The two transverse field components E_x and E_y are the eigenvectors, and the corresponding eigenvalue is $\lambda = -\beta^2$. The dual-core PCF supports two simultaneously excited eigenmodes or supermodes of electric field, one with a symmetric distribution (even mode), and the other with an antisymmetric distribution (odd mode). When only one of cores is illuminated as the fiber input, both modes are equally excited and periodic optical power transfer between the cores along the fiber occurs as a result of beating between the two modes. For instance, Fig. 2 illustrates the

calculated modes of the un-infiltrated dual-core PCF.

Due to the difference between the wavevectors β_{E} of the even mode and β_{O} of the odd mode, there would be a relative phase difference in propagation defined by $\Phi(z)=(\beta_{\mathrm{E}}-\beta_{\mathrm{O}})z$. The coupling length L_C equals the minimum length through which the light energy can be transferred from one core of the dual-core PCF to the second one. This happens for $\Phi(L_C)=\pi$. Hence,

$$L_C=\frac{\pi}{|\beta_{\mathrm{E}}-\beta_{\mathrm{O}}|} \tag{2}$$

Note that, Due to the existence of the two cores in a dual-core PCF, its symmetry becomes twofold, and the degeneracy is removed for *x*- and *y*- polarization modes. As a result, the dual-core PCF becomes birefringent, exhibiting different coupling lengths for either of its orthogonal polarization states. Consequently, there will be four non-degenerate modes, an even and an odd mode for either of its *x* and *y* polarizations.

Another key issue in designing a fiber coupler is to engineer its chromatic dispersion that is responsible for the temporal pulse broadening that limits its transmission bit-rate. In fact, controllability of a PCF chromatic dispersion is a very important issue for practical applications in optical communication systems. The total dispersion (*D*) seen by the fundamental mode of wavelength λ is given by

$$D=\frac{-\lambda}{c}\frac{\mathrm{d}^2\,\mathrm{Re}(n_{\mathrm{eff}})}{\mathrm{d}\lambda^2} \tag{3}$$

where *c* is the velocity of light in free space and $\mathrm{Re}(n_{\mathrm{eff}})$ is the real part of the PCF effective index,

$$n_{\mathrm{eff}}=\frac{\beta}{k_0}=\frac{\beta}{2\pi/\lambda} \tag{4}$$

Parameter β in Eq. (4) includes both the waveguide and the material dispersions.

III. MODELING OF THE PULSE PROPAGATION ACROSS DUAL-CORE PCF

In order to simulate the nonlinear propagation in a dual-core PCF, two coupled generalized nonlinear Schrödinger equations (CG-NLSEs), including most of the standard non-linear phenomena observable in silica fibers such as dispersion, self-phase modulation (SPM), self-steepening (SS) and stimulated Raman scattering (SRS) effects [24], must be solved.

$$\begin{aligned}
&\frac{\partial A_1}{\partial z}+\frac{\alpha}{2}A_1-\sum_{m=2}^{4}\frac{i^{m+1}}{m!}\beta_m^{(1)}\frac{\partial^m A_1}{\partial t^m}\\
&-\sum_{n=0}^{1}\frac{i^{n+1}}{n!}\kappa_n^{(1)}\frac{\partial^n A_2}{\partial t^n}=i\gamma^{(1)}\left(1+\frac{i}{\omega_0}\frac{\partial}{\partial t}\right)\\
&\times A_1(z,t)\int_{-\infty}^{t}R(t-t')\left|A_1(z,t')\right|^2dt'\\
&\frac{\partial A_2}{\partial z}+\frac{\alpha}{2}A_2-\sum_{m=2}^{4}\frac{i^{m+1}}{m!}\beta_m^{(2)}\frac{\partial^m A_2}{\partial t^m}\\
&-\sum_{n=0}^{1}\frac{i^{n+1}}{n!}\kappa_n^{(2)}\frac{\partial^n A_1}{\partial t^n}=i\gamma^{(2)}\left(1+\frac{i}{\omega_0}\frac{\partial}{\partial t}\right)\\
&\times A_2(z,t)\int_{-\infty}^{t}R(t-t')\left|A_2(z,t')\right|^2dt'
\end{aligned} \tag{5}$$

where $A_j\,(j=1,2)$ is the electric field envelope in the j-th core, *z* is axial propagation distance, and *t* is the time. The envelopes of input pulses launched into the dual-core PCF cores at *z*=0 are assumed to be of the form of

$$\begin{aligned}
&A_1(z=0,T)=\sqrt{P_0}\,\mathrm{Sech}\left(\frac{T}{T_0}\right),\\
&A_2(z=0,T)=0
\end{aligned} \tag{6}$$

where P_0, T_0, and T denote the pulse peak power, width and retarded time, repectively. In Eq. (5), parameter α denotes the linear propagation loss, β_{m} represent the dispersion coefficients of order *m* associated with the Taylor series expansion of the propagation

constant $\beta(\omega)$ about the carrier frequency, ω_0 ,

$$\beta_m = \left(\frac{d^m \beta}{d\omega^m} \right)_{\omega=\omega_0} \quad m = 2, 3, \text{ and } 4 \tag{7}$$

in which β_2 is the second order dispersion coefficient that is related to GVD parameter by $\beta_2 = -\left(\lambda^2 / 2\pi c\right) \times D$. This effect becomes considerable when the fiber length is comparable or longer than the so called "dispersion length" defied by $L_D = T_0^{\,2} / \left|\beta^2\right|$. Higher orders dispersion terms become dominant when the input pulse center wavelength (λ_c) is near the zero GVD wavelength or when the bandwidth of the pulse becomes comparable to the center frequency (or for ultra-short pulses of widths $T_0 < 1$ ps). Coefficients κ_n are defined by

$$\kappa_n = \left(d^n \kappa / d\omega^n \right)_{\omega=\omega_0} \quad n = 0, 1 \tag{8}$$

in which $\kappa = \left(\beta_E - \beta_0\right)/2 = \pi/\left(2L_C\right)$ is the frequency dependent coupling coefficient, related to the even and odd propagation constant, the coupling constant κ_0 is due to the spatial overlap of the modes of the two waveguides and is responsible for the periodic exchange of the power between the two cores with a period of $\pi/\kappa_0 = 2L_C$, and κ_1 is the dispersive part of the coupling coefficient. It has been shown that, in dual-core fibers of lengths comparable to or longer than the so called "walk-off length" defined by $L_W = T_0/\left|\kappa_1\right|$, the term κ_1 can break-up the input pulses and is negligible otherwise [25]. Parameter $\gamma = n_2\omega_0/\left(cA_{\text{eff}}\right)$, on the right hand sides of Eqs. (5), represents the nonlinear coefficient for either of two cores, in which n_2 is the nonlinear Kerr index of the silica, and A_{eff} is the corresponding effective mode area. The response function $R(t)$ in the integrand of the integral on the right hand sides of Eq. (5) can be written in the form of:

$$R(t) = (1 - f_R)\,\delta(t) + f_R h_R(t) \tag{9}$$

where $\delta(t)$ is the Dirac delta function, and $h_R(t)$ represents the Raman contribution from the Raman gain spectrum, and f_R is found by normalizing $h_R(t)$,

$$\int_0^\infty h_R(t)\,dt = 1 \tag{10}$$

Note that for the input pulses under study, the cross-phase modulation (XPM) is insignificant and hence, the corresponding terms do not appear in Eqs. (5)

IV. Coupler Engineering by Means of Infiltration

In this section, we employ the selective microfluidic infiltration approach, similar to the one recently proposed elsewhere [20] in engineering the PCFs dispersion profiles, to engineer the dispersion and hence coupling characteristics of the dual-core PCF under study.

In doing so, we have considered two selective infiltration schemes. Figure 1(a) illustrates the un-infiltrated part of the dual-core PCF of Fig. 1 surrounded by the rectangle. Figures 1(b) and 1c represent the two infiltration schemes. The white circles represent the un-infiltrated air-holes and the colored (dark) circles surrounding the two dual-core PCF cores symbolize the infiltrated ones. As observed from these two figures, the only difference between the two schemes is the air-hole separating the two dual-core PCF cores that is un-infiltrated in the scheme represented by Fig. 1(b) while infiltrated by the scheme depicted in Fig. 1(c). The fluid refractive index is assumed to be the same as that we used in [20]; i.e. $n_F = 1.3$. Now, we investigate the role of these microfluidic infiltrations on the dual-core PCF dispersion profile, D, and its coupling length, L_C. Feasibility of microfluidic infiltration into PCFs longer than several centimeters have already been demonstrated experimentally [17]. On the other hand, finite length of every PCF

considered in this study is more than two orders of magnitude larger than its effective core radius. Hence, assumption of infinitely long PCFs for characterizing such PCFs is mathematically justified.

First, we compare the electric field distributions for the fundamental modes of the un-infiltrated and infiltrated dual-core PCFs. Top views of these *E*-field distributions for *x*- and *y*-polarized even and odd modes, with center wavelength of $\lambda_c = 1550$ nm, are compared in Fig. 3. The distribution illustrated by Fig. 3(a) belongs to the un-infiltrated case depicted by Fig. 1(a), and those depicted in Figs. 3(b), and (c) belong to infiltrated scheme represented by Fig. 1(b) and (c), respectively. Each even mode is depicted by a pair of lighter (yellowish) distributions centered with white spots as their peaks both directed along +z-direction. Each of the odd modes are, on the other hand, represented by a positively directed lighter distribution plus a darker (reddish) distribution with a black spot on the center depicting its peak directed along –*z*-direction. The horizontal and vertical arrows display distributions corresponding to the *x*- and *y*- polarized *E*-fields, respectively. The comparison shows that due to the higher effective index of the infiltrated dual-core PCF, the corresponding field distributions expand to the cladding regions.

Moreover, infiltration of the air-hole separating the two cores leads to a stronger overlap of the modal fields between the two adjacent cores. We expect this overlap to enhance the corresponding coupling characteristics.

Next, we calculate and compare the wavelength dependence of the effective refractive indices, the GVD parameters, *D*, and coupling lengths, for the *x*-polarized even supermodes propagating along the three dual-core PCFs on Fig. 1, as illustrated in Fig. 4.

In this figure the dotted curve, in each part, represents the variation of the corresponding characteristics as a function of the wavelength λ for the un-infiltrated case of Fig. 1(a), while the solid and the dashed curves represent the corresponding characteristics for infiltrated schemes of Fig. 1(b) and (c), respectively. As shown in Fig. 4, microfluidic infiltration has increased the effective refractive index and reduced the coupling length, in general.

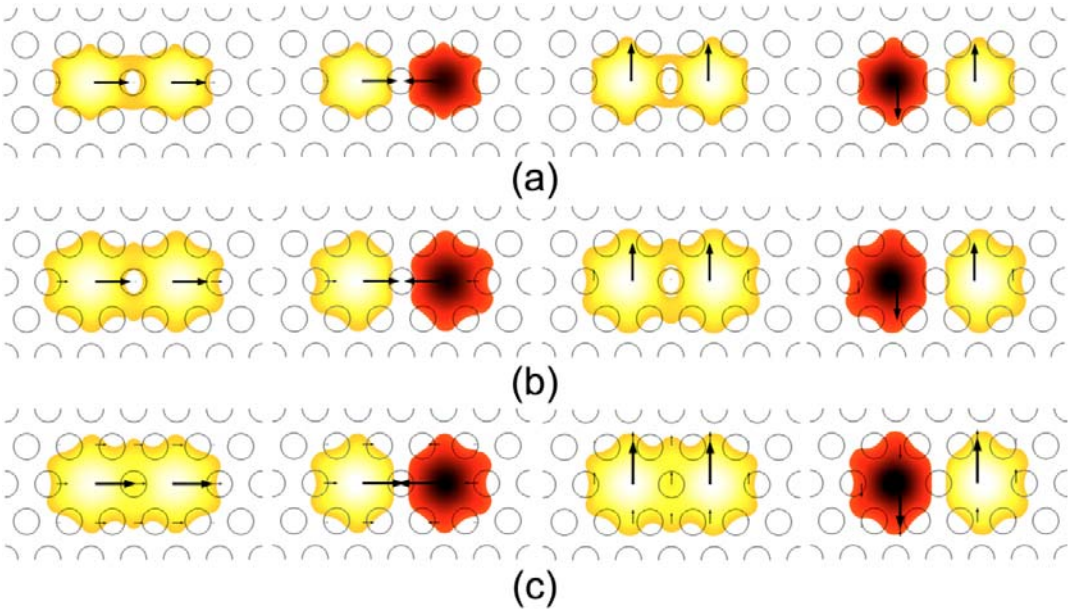

Fig. **3** Electric field distributions, from left to right: the *x*-polarized even mode, *x*-polarized odd mode, *y*-polarized even mode, and the *y*-polarized odd mode for (a) un-infiltrated, (b) infiltrated as in Fig. 1(b), and (c) infiltrated as in Fig. 1(c) dual-core PCFs, all with center wavelengths of $\lambda_c = 1550$ nm. The arrows depict the direction of the corresponding *E*-fields.

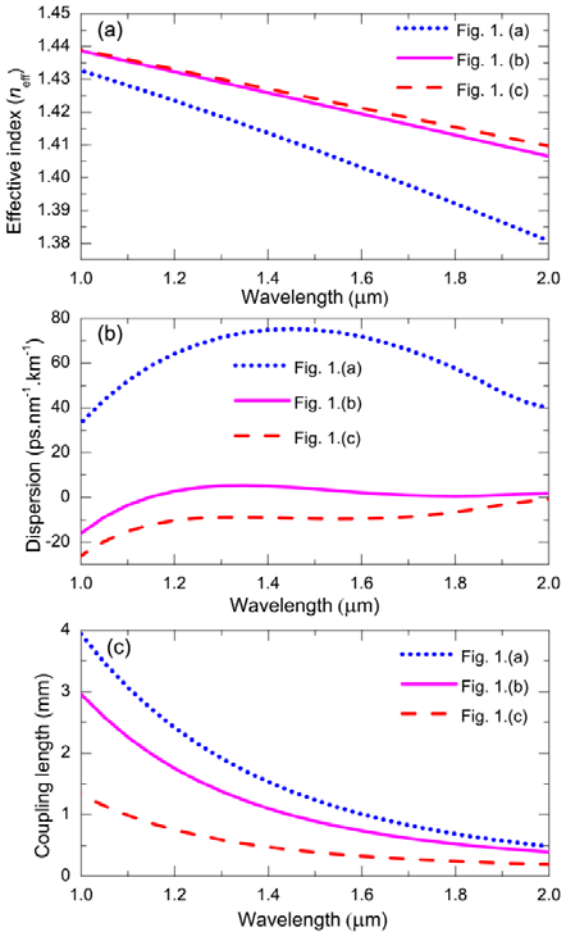

Fig. 4 Comparison of the (a) effective refractive indices, (b) dispersion profiles, and (c) coupling lengths of *x*-polarized even supermodes propagating along the three dual-core PCFs of Figs. 1(a) (dotted curves), 1(b) (solid curves), and 1c (dashed curves).

Figure 4(a) shows that the fluid effect at shorter wavelengths due to the greater influence of material dispersion is not prominent. However, at longer wavelengths, this effect strongly appeared. Furthermore, as expected from the field distribution, infiltration of the middle air-hole separating the dual-core PCF cores increases n_{eff} further and hence reduces L_C more. Figure 4(b) shows that the infiltration scheme represented by Fig. 1(b) results in a nearly zero and flattened dispersion across a wide range of wavelengths $1.2\ \mu\text{m} < \lambda < 2\ \mu\text{m}$ (i.e, width of 0.8 μm in the ITU region), covering O (1260–1360 nm), E (1360–1460 nm), S (1460–1530 nm), C (1530–1565 nm), L (1565–1625 nm), and U (1625–1675 nm) telecommunication wavelength bands. Figure 4(b) also shows that by infiltrating the middle air-hole, the sign of dispersion changes to the negative value.

V. Results and Discussion

In this Section, using symmetrized split step Fourier method (SSFM), we study the role of microfluidic infiltration approach to design all-optical devices based on dual-core PCF. As discussed earlier for solving the GC-NLSEs, the values of high order dispersion, coupling coefficients, and nonlinear parameter are needed. We plot these parameters for the different cases of Fig. 1 as function of wavelength in Figs. 5-7. Figure 5 illustrates the variation of β_2, β_3, and β_4 versus wavelength for mentioned cases. From this figure it can be seen that, magnitude of $|\beta_2|$, $|\beta_3|$, and $|\beta_4|$ for the infiltrated cases of Fig. 1 (b) and (c) significantly reduces. In addition, it

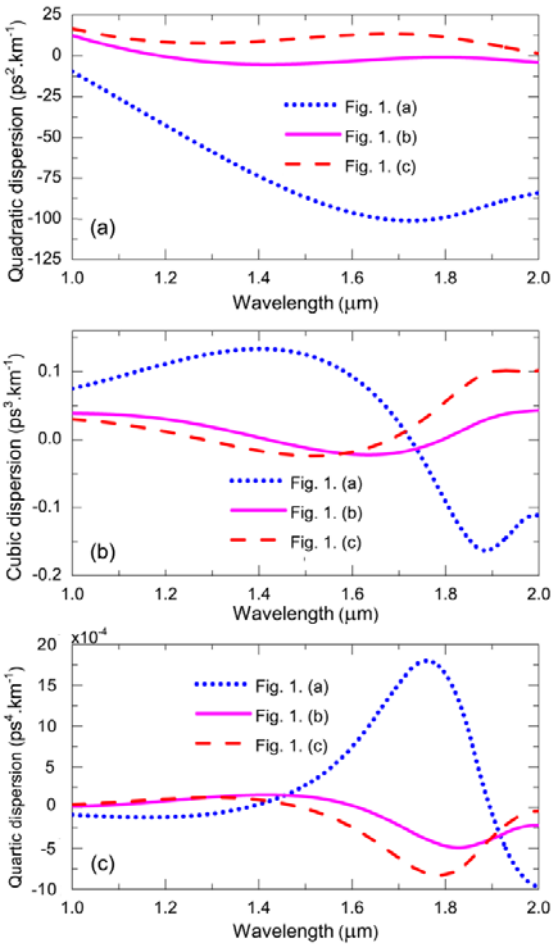

Fig. **5** Comparison of the (a) β_2, (b) β_3, and (c) β_4 profiles of *x*-polarized even supermode for the conventional and engineered dual-core PCFs.

shows that the sign of β_2 varies from normal to anomalous dispersion by infiltrating the middle air-hole. Dispersion engineering has diverse application in nonlinear optics area. For instance, it has been recently demonstrated that phase matched nonlinear processes like FWM are strongly dependent on the sign of the β_2 and β_4.

Figure 6 illustrates the calculated coupling coefficient (κ_0) and coupling coefficient dispersion (κ_1) profiles versus wavelength. It shows that infiltrating the air-holes of dual-core PCF, increases the value of κ_0 and κ_1, simultaneously. In following, we will discuss the effects of coupling coefficient dispersion upon pulse propagation.

Dependencies of the effective mode area, A_{eff}, and nonlinear parameter, γ, on the operating wavelength (λ) are depicted in Fig. 7. Figure 7(a) shows that by increasing wavelength the effective mode area for all three cases increases and consequently, the nonlinear parameter will be reduced. As expected, the effective mode area for the infiltrated PCF of Fig. 1(c) is larger than the un-infiltrated dual-core PCF of Fig. 1(a). Moreover, the rates of increase in A_{eff} with wavelength for both infiltrated dual-core PCFs are twice as much larger than the rate of increase for the un-infiltrated one. On the other hand, Fig. 7(b) shows that as wavelength increases γ decreases for all three cases, under study, while γ for dual-core PCFs of Figs. 1(a) and (c) are the largest and smallest, respectively. Using the SSFM, Eq. (5) was solved with the dual-core PCF taken from Figs. 5-7 at center wavelength of λ_c=1550 nm, and are summarized in Table 1.

The input signals launched into "A" and "B", as bar and cross ports are, respectively $A_1(z=0,T)$ and $A_2(z=0,T)$ given by Eq. (6), with P_0=100 W, T_0=100 fs, and λ=1550 nm. The results are illustrated in Fig. 8. This figure compares both temporal and spectral evolutions of signals propagating along cores "A" and "B" of 5-mm long dual-core PCFs.

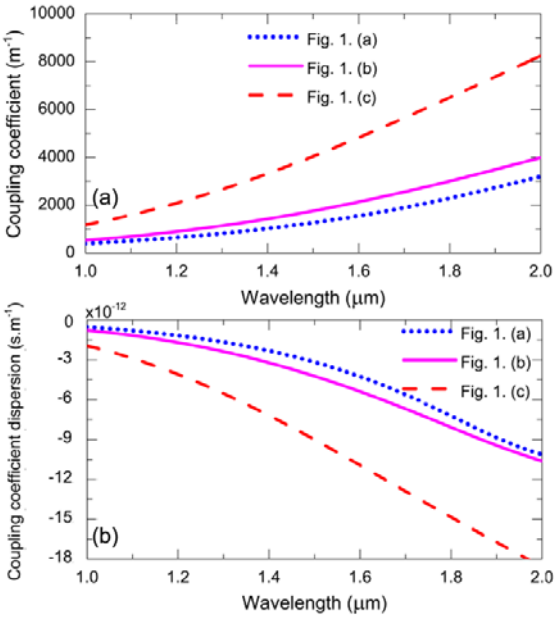

Fig. **6** Comparison of the (a) coupling coefficient and (b) coupling coefficient dispersion of *x*-polarized even supermode for the conventional and engineered dual-core PCF of Fig. 1.

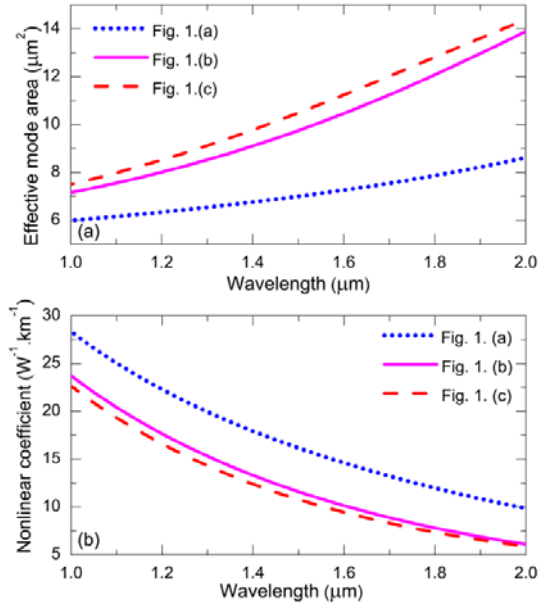

Fig. **7** Comparison of the (a) effective mode area and (b) nonlinear parameter of *x*-polarized even supermode for the three dual-core PCFs of Fig. 1.

As seen from this figure, input pulse continues to travel through the same core, before it couples to the adjacent core. The coupling lengths for all three dual-core PCFs of Fig. 1 are given in Table 2.

Table **1** Parameters extracted from Figs. 5-7, at λ_c=1550 nm, used in solving Eqs. (5)

		Value in 1550 nm			
Parameter	Symbol	Fig. 1(a)	Fig. 1(b)	Fig. 1(c)	unit
Coupling length	L_C	1.11	0.808	0.354	mm
Coupling coefficient	κ_0	1408.82	1945.81	4433.72	m^{-1}
Coupling coefficient dispersion	κ_1	−3.69	−4.79	−9.97	$ps.m^{-1}$
Dispersion	D	73.68	2.96	−9.66	$ps.\ nm^{-1}.km^{-1}$
Quadratic dispersion	β_2	−86.88	−4.098	11.92	$ps^2.km^{-1}$
Cubic dispersion	β_3	1.24×10^{-1}	-1.79×10^{-2}	-2.29×10^{-2}	$ps^3.km^{-1}$
Quadretic dispersion	β_4	2.77×10^{-4}	9.29×10^{-4}	-1.09×10^{-5}	$ps^4.km^{-1}$
Effective mode area	A_{eff}	7.12	10.09	10.85	μm^2
Nonlinear coefficient	γ	12.50	10.83	8.20	$W^{-1}.km^{-1}$

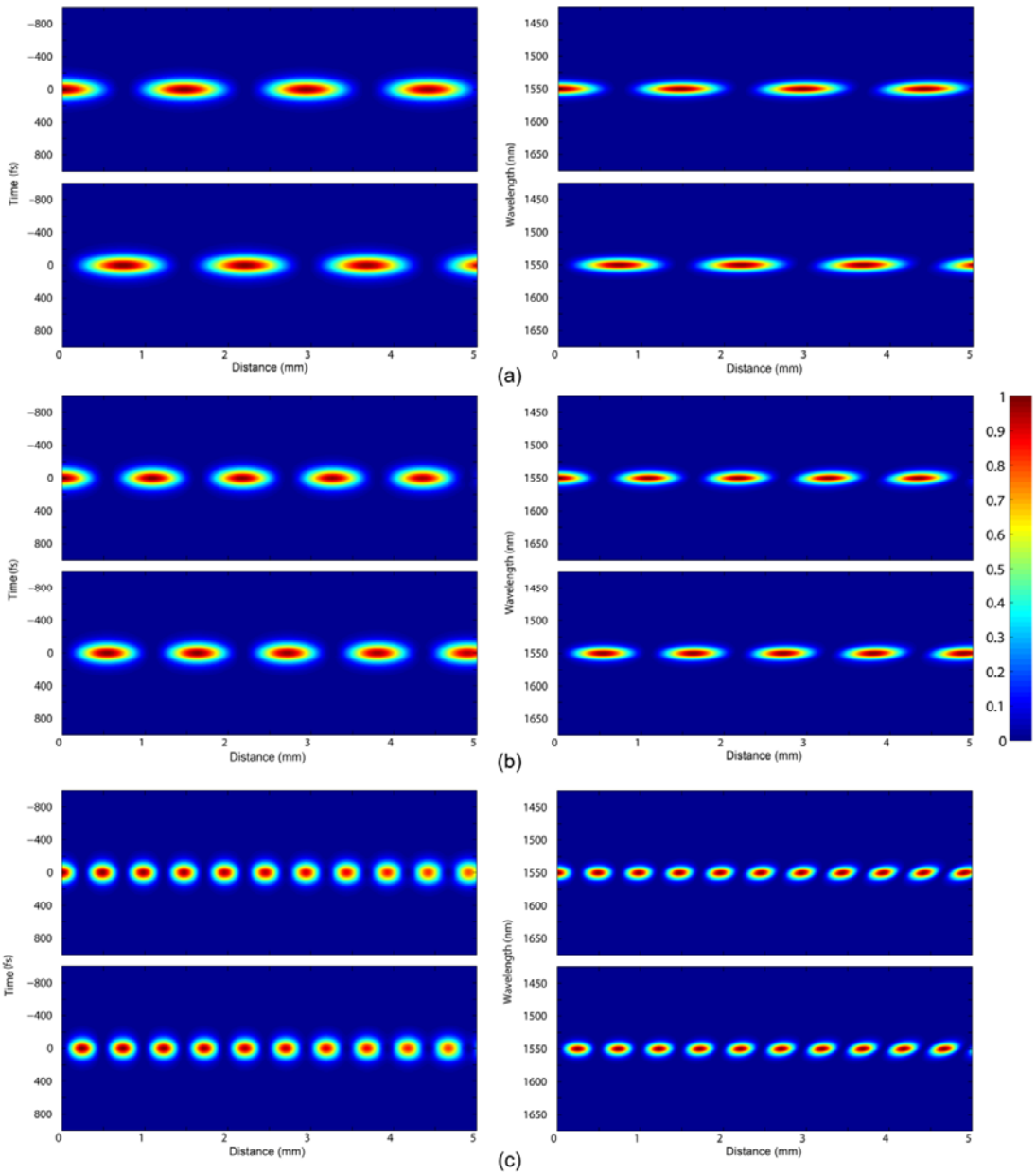

Fig. **8** Temporal (left) and spectral (right) evolutions of light signals propagating along cores “A” and “B” of 5-mm long dual-core PCFs of (a) Fig. **1**a, (b) Fig. **1**b, and (c) Fig. **1**c, for P_0=100 W, T_0=100 fs and λ_c=1550 nm.

Table **2** Compression of L_C, L_D, L_W in dual-core PCFs of Fig. **1** for P_0=100 W, T_0=100 fs, and λ_c=1550 nm

Parameter	Value in 1550 nm			unit
	Fig. 1(a)	Fig. 1(b)	Fig. 1(c)	
L_C	1.11	0.808	0.354	mm
L_D	115.08	2440.21	838.37	mm
L_W	27.07	20.84	10.025	mm

The results presented in Table 2 show that the fluid infiltration has reduced the coupling length by a factor of three, enabling the design of compact dual-core PCFs. Moreover, these figures show that the pulse width remains intact during propagation. This is due to the fact that the coupling lengths are shorter than the dispersion lengths (i.e., $L_C \ll L_D$). The corresponding dispersion lengths that are also significantly larger than the fiber lengths as well are compared in Table 2. Another parameter that is also compared for the three dual-core PCFs, in this table, is the walk-off length (L_W), which is also significantly larger than the corresponding coupling length. Moreover, from Fig. 8 (c) it is observed that at z=4 mm amplitude of the pulse start to reduce. This phenomenon is occurred due to increasing coupling coefficient dispersion. Data presented in Table 2 also show that dual-core PCF of Fig. 1(c) suffers from a large $|\kappa_1|$ value that leads to the shortest walk-off length, among all three cases, for the given input pulse width. Nevertheless, the ratio $L_W/L_C = 28.32$ for this infiltrated dual-core PCF happens to be largest of all, while these ratios for Fig. 1(b) and 1(a) are, respectively, 25.79 and 24.39. Next we investigate the dependence of ratios L_D/L_C and L_W/L_C on the pulse width (T_0) for all three PCFs, as illustrated in Fig. 9. The comparison, illustrated in this figure, reveals that infiltration of holes surrounding both fiber cores increases the ratio of L_D/L_C by more than an order of magnitude, for any given pulse width in the range of 10 fs $< T <$ 300 fs. Whereas, the effect of infiltration on the ratio of L_W/L_C is not as significant. Nevertheless, Fig. 9 (b) reveals that for $T_0 > 30$ fs for which $L_W/L_C > 10$ and $L_D/L_C > 100$, large values

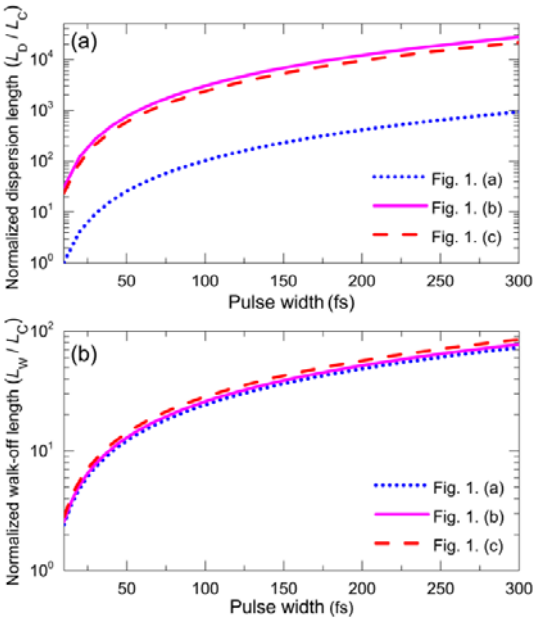

Fig. **9** Dependencies of the normalized (a) dispersion length, L_D/L_C, and (b) walk-off length, L_W/L_C, of x-polarized even supermode on the pulse width (T_0) for dual-core PCFs of Fig. 1.

of $|\kappa_1|$ does not limit the design of couplers of lengths $L \lesssim L_W$.

Then by considering 50-mm long PCFs, we try to shed more light on the effect of the size of $|\kappa_1|$ on the pulse propagation, while the other parameters are kept constant. Figure 10 compares both temporal and spectral evolutions of an optical pulse of $P_0 = 100$ W, $T_0 = 100$ fs and $\lambda = 1550$ nm, propagating along cores "A" and "B" of 50-mm long dual-core PCFs of Fig. 1. Going from (a) to (b) and then to (c), $|\kappa_1|$ increases as tabulated in Table 1. This increase causes the signal, after traversing a distance along each dual-core PCF almost equal to its corresponding walk-off length, to split completely into two pulses in the time domain, each walking-off the respective core. This splitting effect is manifested by a twist about the center wavelength in the spectral evolution, splitting the light pulse to a slow and a fast branch [26].

As one can see from these figures, the separation between two temporal pulses, linearly increases with distance along the PCF.

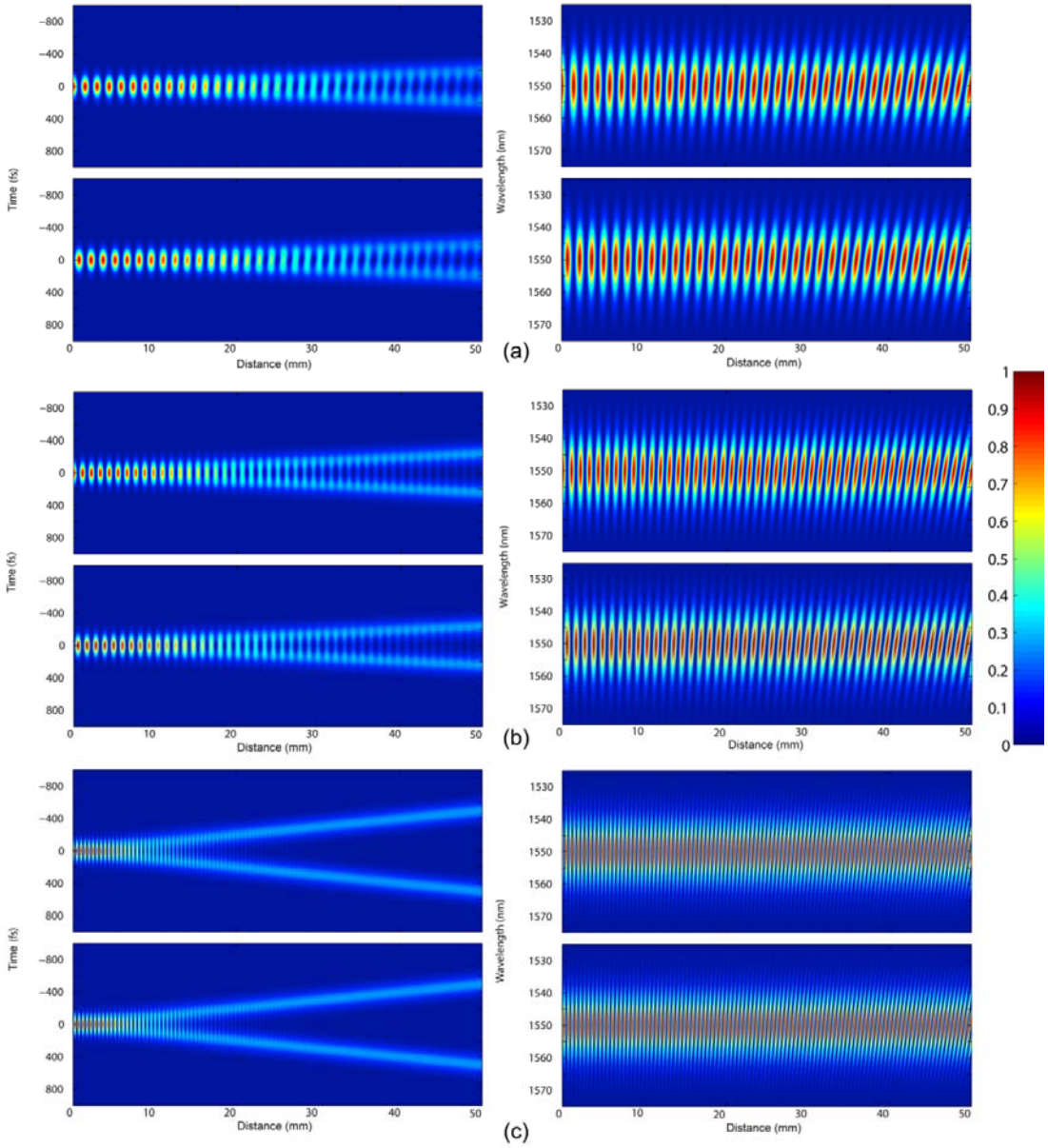

Fig. **10** Temporal (left) and spectral (right) evolutions of light signals propagating along cores "A" and "B" of 50-mm long dual-core PCFs of (a) Fig. **1**a, (b) Fig. **1**b, and (c) Fig. **1**c, for P_0=100 W, T_0=100 fs and λ_c=1550 nm.

One could relate this separation and coupling coefficient dispersion by following derivation. For a dual-core PCF of length L, group delays for each supermode propagating along a unit length of the dual-core PCF is given by [27]

$$\tau_{E/O} = \frac{d\beta_{E/O}}{d\omega} \tag{11}$$

Consequently, the group delay difference, $\Delta\tau$, per fiber unit length is

$$\Delta\tau = \tau_E - \tau_O = 2\frac{d\kappa_0}{d\omega} = 2\kappa_1 \tag{12}$$

Equation (12) provides a physical meaning for coupling coefficient dispersion. The two pulses, corresponding to the two fundamental modes of the dual-core PCF, walk-off while the input pulse duration is shorter than the group delays difference, $\Delta\tau \times L$. In this case, the coupling coefficient dispersion in the fiber cause serious pulse distortion or even pulse break-up. In fact, for 50-mm long dual-core

PCFs of Figs. 1(a), (b), and (c) the group delays differences are 369, 479, and 997 fs that are longer than the input pulse duration of 100 fs. An important parameter in this case is the peak-to-peak spectral separation, $\Delta\lambda$, can cover a wide range by adjusting the PCF length. The group delay difference $\Delta\tau$ and the spectral separation of the transmission peaks $\Delta\lambda$ are related by $\Delta\tau = \lambda^2/(c\Delta\lambda L)$ [28]. The spectral dependence of $\Delta\lambda$ and corresponding $|\Delta\tau|$ for 200-mm long PCFs are plotted in Fig. 11.

A recent experiment [28] took advantage of the pulse break-up effect to generate high repetition rate pulse trains, using a 480-mm long fiber with a strong coupling coefficient dispersion of ~10 ps/m was used. Figure 11 shows that a similar effect can be observed in dual-core PCFs under study.

VI. CONCLUSION

We have proposed a novel microfluidic infiltrated dual-core PCF coupler with nearly zero and ultra-flattened dispersion across a wide wavelength. Through numerical simulations, it was shown that by infiltrating air-holes in the cladding, the coupling length could be reduced considerably. The numerical simulation results indicate the possibility of realizing couplers with coupling lengths less than 0.36 mm at 1.55 μm.

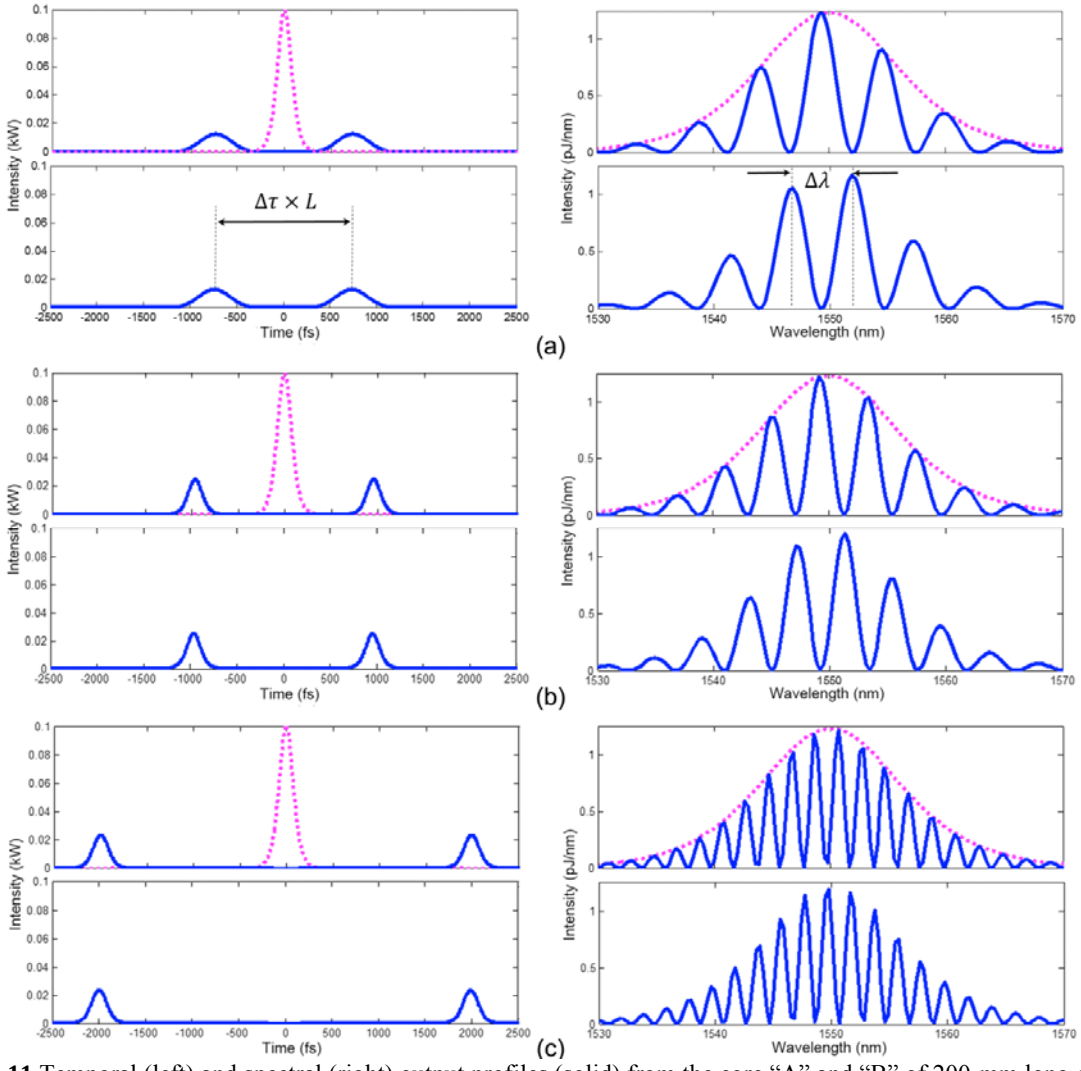

Fig. **11** Temporal (left) and spectral (right) output profiles (solid) from the core "A" and "B" of 200-mm long dual-core PCFs of (a) Fig. **1**a, (b) Fig. **1**b, and (c) Fig. **1**c, for input pulse pump of P_0=100 W, T_0=100 fs (dotted) and λ_c=1550 nm.

It is also revealed that by properly infiltrating the air holes of the PCFs ultra flattened dispersion profile can be achieved. We study the pulse break-up due to the walk-off length and took advantage of pulse break-up effect to generate pulse trains with high repetition rate.

REFERENCES

[1] J. Knight, T. Birks, P. S. J. Russell, and D. Atkin, "All-silica single-mode optical fiber with photonic crystal cladding," Opt. Lett., vol. 21, pp. 1547-1549, 1996.

[2] P. S. J. Russell, "Photonic-crystal fibers," J. Lightwave Technol., vol. 24, pp. 4729-4749, 2006.

[3] A. Betlej, S. Suntsov, K. Makris, L. Jankovic, D. Christodoulides, G. Stegeman, J. Fini, R. Bise, and D. DiGiovanni, "All-optical switching and multifrequency generation in a dual-core photonic crystal fiber," Opt. Lett., vol. 31, pp. 1480-1482, 2006.

[4] K. R. Khan and T. X. Wu, "Short pulse propagation in wavelength selective index-guided photonic crystal fiber coupler," IEEE J. Sel. Topics Quantum Electron., vol. 14, pp. 752-757, 2008.

[5] K. R. Khan, T. X. Wu, D. N. Christodoulides, and G. I. Stegeman, "Soliton switching and multi-frequency generation in a nonlinear photonic crystal fiber coupler," Opt. Express., vol. 16, pp. 9417-9428, 2008.

[6] T. Uthayakumar, R. Raja, and K. Porsezian, "All-Optical Steering of Light Through Nonlinear Twin-Core Photonic Crystal Fiber Coupler at 850 nm," J. Lightwave Technol., vol. 30, pp. 2110-2116, 2012.

[7] K. Saitoh, Y. Sato, and M. Koshiba, "Coupling characteristics of dual-core photonic crystal fiber couplers," Opt. Express., vol. 11, pp. 3188-3195, 2003.

[8] K. Saitoh, Y. Sato, and M. Koshiba, "Polarization splitter in three-core photonic crystal fibers," Opt. Express., vol. 12, pp. 3940-3946, 2004.

[9] K. Saitoh, N. J. Florous, and M. Koshiba, "Design of narrow band-pass filters based on the resonant-tunneling phenomenon in multi-core photonic crystal fibers," Opt. Express., vol. 13, pp. 10327-10335, 2005.

[10] D. Chen, G. Hu, and L. Chen, "Dual-core photonic crystal fiber for hydrostatic pressure sensing," IEEE Photon. Technol. Lett., vol. 23, pp. 1851-1853, 2011.

[11] S. K. Varshney, N. J. Florous, K. Saitoh, and M. Koshiba, "The impact of elliptical deformations for optimizing the performance of dual-core fluorine-doped photonic crystal fiber couplers," Opt. Express., vol. 14, pp. 1982-1995, 2006.

[12] Y. Yue, G. Kai, Z. Wang, C. Zhang, Y. Lu, Y. Li, T. Sun, L. Jin, J. Liu, and Y. Liu, "Broadband single-polarization single-mode photonic crystal fiber coupler," IEEE Photon. Technol. Lett., vol. 18, pp. 2032-2034, 2006.

[13] M. Ebnali-Heidari, C. Monat, C. Grillet, and M. Moravvej-Farshi, "A proposal for enhancing four-wave mixing in slow light engineered photonic crystal waveguides and its application to optical regeneration," Opt. Express., vol. 17, pp. 18340-18353, 2009.

[14] M. Bitarafan, M. Moravvej-Farshi, and M. Ebnali-Heidari, "Proposal for postfabrication fine-tuning of three-port photonic crystal channel drop filters by means of optofluidic infiltration," Appl. Opt., vol. 50, pp. 2622-2627, 2011.

[15] S. Bakhshi, M. K. Moravvej-Farshi, and M. Ebnali-Heidari, "Design of an ultracompact low-power all-optical modulator by means of dispersion engineered slow light regime in a photonic crystal Mach–Zehnder interferometer," Appl. Opt., vol. 51, pp. 2687-2692, 2012.

[16] M. Ebnali-Heidari, C. Grillet, C. Monat, and B. Eggleton, "Dispersion engineering of slow light photonic crystal waveguides using microfluidic infiltration," Opt. Express., vol. 17, pp. 1628-1635, 2009.

[17] M. Vieweg, T. Gissibl, S. Pricking, B. Kuhlmey, D. Wu, B. Eggleton, and H. Giessen, "Ultrafast nonlinear optofluidics in selectively liquid-filled photonic crystal fibers," Opt. Express., vol. 18, pp. 25232-25240, 2010.

[18] C. Yu and J. Liou, "Selectively liquid-filled photonic crystal fibers for optical devices," Opt Express., vol. 17, pp. 8729-8734, 2009.

[19] K. Nielsen, D. Noordegraaf, T. Sørensen, A. Bjarklev, and T. P. Hansen, "Selective filling

of photonic crystal fibres," Journal of Optics A: Pure and Appl. Opt., vol. 7, L13, 2005.

[20] M. Ebnali-Heidari, F. Dehghan, H. Saghaei, F. Koohi-Kamali, and M. Moravvej-Farshi, "Dispersion engineering of photonic crystal fibers by means of fluidic infiltration," J. Mod. Opt., vol. 59, No. 16, pp. 1384–1390, 2012.

[21] F. Koohi-Kamali, H. Saghaei, M. Ebnali-Heidari, and M. K. Moravvej-Farshi, "Supercontinuum generation through honey-comb photonic crystal fiber in visible spectral region," 20th Iranian Conference on Electrical Engineering (ICEE2012), Tehran, Iran, 2012.

[22] F. Koohi-Kamali, H. Saghaei, M. Ebnali-Heidari, and M. K. Moravvej-Farshi, "Design of double-core photonic crystal fiber coupler by means of optofluidic infiltration," The 19th Iranian Conference on Optics and Photonics (ICOP2013), Zahedan, Iran, 2013.

[23] K. Saitoh and M. Koshiba, "Full-vectorial imaginary-distance beam propagation method based on a finite element scheme: Application to photonic crystal fibers," IEEE J. Quanum Electron., vol. 38, pp. 927-933, 2002.

[24] G. P. Agrawal, "Nonlinear Fiber Optics," 3rd ed., New York: Academic Press, 2001.

[25] M. Liu and K. Chiang, "Propagation of ultrashort pulses in a nonlinear two-core photonic crystal fiber," Appl. Phys. B: Lasers and Optics., vol. 98, pp. 815-820, 2010.

[26] M. Ebnali-Heidari, M. K. Moravvej-Farshi, and A. Zarifkar, "Multichannel wavelength conversion using fourth-order soliton decay," J. Lightwave Technol., vol. 25, pp. 2571-2578, 2007.

[27] K. S. Chiang, "Intermodal dispersion in two-core optical fibers," Opt. Lett., vol. 20, pp. 997-999, 1995.

[28] P. Peterka, P. Honzatko, J. Kanka, V. Matejec, and I. Kasik, "Generation of high-repetition-rate pulse trains in a fiber laser through a twin-core fiber," in Proceedings of SPIE, pp. 376-381,2003.

Farshid Koohi-Kamali was born in Shahrekord, Iran, in 1985. He received the B.Sc. degree from Shahrekord University, and the M.Sc. degree from IAU, Sciences and Research Branch, at Tehran, in 2010 and 2013, respectively, all in electrical engineering. Farshid has been working on numerical modeling and simulation of nonlinear effects in photonic crystal fibers. His current research interests include photonic crystal fibers, nonlinear optics, slow light, and fiber optical sensors.

Majid Ebnali-Heidari (M'2007) graduated with a BS in Electrical Engineering from Isfahan University of Technology, 2003, and Ms , and PhD in Electrical Engineering, both from Tarbiat Modares University, in 2005, 2009 respectively. From 2008 to 2009, he was visiting student at the Centre for Ultrahigh-bandwidth Devices for Optical Systems (CUDOS), School of Physics at the University of Sydney, Australia, where he was engaged in the optofluidics slow light research area with the slow light CUDOS flagship project.

Now, he is a faculty member of the Sharekord University. His fields of interests are applications of nonlinear optics in photnics, slow light, photonic crystal, and optofluidic devices.

Mohammad Kazem Moravvej-Farshi (was born in Yazd, Iran, in 1952. He received the B. Sc. and the M. A. degrees in physics from Sharif University of Technology (SUT), Tehran, Iran, in 1976, and the University of Southern California (USC), Los Angeles, California, in 1978, respectively, the M. Sc. and the Ph. D degrees in electronics from the University of California at Santa Barbara (UCSB), in 1980, and the University of New South Wales (UNSW), Sydney, Australia, in 1987, respectively. From 1980 to 1984, he was a member of research staff with the Division of Microwave, Iran Telecommunication Research Center (ITRC). He joined Tarbiat Modares University (TMU) in 1987, where he is currently a Professor of Electronics and head of the Advanced Device Simulation Lab (ADSL). His current fields of interest are designing and simulation of all-optical devices based on non-linear phenomena, Photonic Crystals and nanostructures; and graphene and CNT based. nanophotonic and nanoelectronic devices.

Professor Moravvej Farshi is currently a senior member of IEEE and a senior member of the Optical Society of America (OSA). He is also one of the founders of the Optics and Photonics Society of Iran.